Nano Research
DOI 10.1007/s12274-014-0680-z
Research Article
ISSN 1998-0124
CN 11-5974/O4

Benchtop aqueous two-phase extraction of isolated individual single-walled carbon nanotubes.

Navaneetha K. Subbaiyan,[1,†] A. Nicholas G. Parra-Vasquez, [1,†] Sofie Cambré,[1,2,†] Miguel A. Santiago Cordoba,[1] Sibel Ebru Yalcin,[1] Christopher E. Hamilton,[1] Nathan H. Mack,[1] Jeffrey L. Blackburn,[3] Stephen K. Doorn,[1] and Juan G. Duque[1](✉).

Nano Res., **Just Accepted Manuscript** • DOI: 10.1007/s12274-014-0680-z
http://www.thenanoresearch.com on December 8 2014

Just Accepted

TSINGHUA UNIVERSITY PRESS Springer

Template for Preparation of Manuscripts for *Nano Research*

This template is to be used for preparing manuscripts for submission to *Nano Research*. Use of this template will save time in the review and production processes and will expedite publication. However, use of the template is not a requirement of submission. Do not modify the template in any way (delete spaces, modify font size/line height, etc.). If you need more detailed information about the preparation and submission of a manuscript to Nano Research, please see the latest version of the Instructions for Authors at http://www.thenanoresearch.com/.

TABLE OF CONTENTS (TOC)

Benchtop aqueous two-phase extraction of isolated individual single-walled carbon nanotubes

Navaneetha K. Subbaiyan, A. Nicholas G. Parra-Vasquez, Sofie Cambré, Miguel A. Santiago Cordoba, Sibel Ebru Yalcin, Christopher E. Hamilton, Nathan H. Mack, Jeffrey L. Blackburn, Stephen K. Doorn, and Juan G. Duque*

Los Alamos National Laboratory, USA
University of Antwerp, Belgium
National Renewable Energy Laboratory, USA

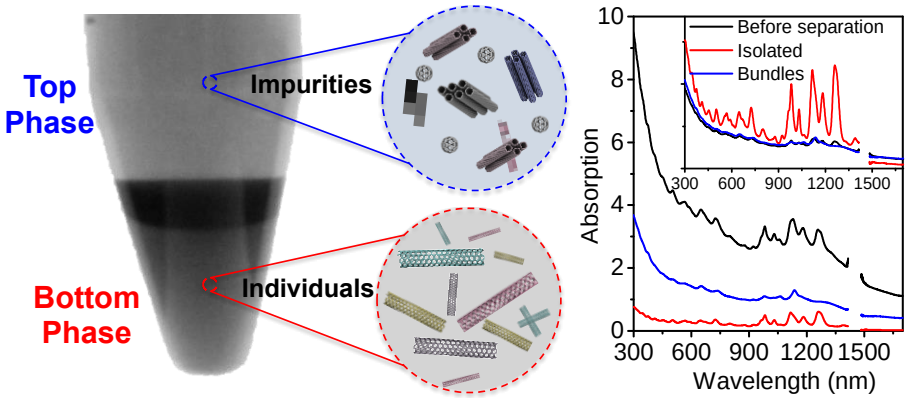

A practical, fast and scalable benchtop aqueous-two-phase extraction of isolated individual single-walled carbon nanotubes from bundles and impurities in aqueous dispersions is presented.

Provide the authors' website if possible.
http://www.lanl.gov/expertise/profiles/view/juan-duqe

Nano Research
DOI (automatically inserted by the publisher)
Research Article
ISSN 1998-0124
CN 11-5974/O4

Benchtop aqueous two-phase extraction of isolated individual single-walled carbon nanotubes.

Navaneetha K. Subbaiyan,[1,†] A. Nicholas G. Parra-Vasquez, [1,†] Sofie Cambré,[1,2,†] Miguel A. Santiago Cordoba,[1] Sibel Ebru Yalcin,[1] Christopher E. Hamilton,[1] Nathan H. Mack,[1] Jeffrey L. Blackburn,[3] Stephen K. Doorn,[1] and Juan G. Duque[1](✉).

[1] *Chemistry Division, Physical Chemistry and Applied Spectroscopy Group (C-PCS), Center for Integrated Nanotechnologies (CINT), and Materials Science & Technology Division (MST-7), Los Alamos National Laboratory, Los Alamos, New Mexico 87544, United States.* [2] *Experimental Condensed Matter Physics Laboratory, University of Antwerp, Antwerp, B-2610, Belgium*

[3] *National Renewable Energy Laboratory, Golden, Colorado 80401, United States*

[†] *These authors contributed equally*

Received: day month year
Revised: day month year
Accepted: day month year (automatically inserted by the publisher)

KEYWORDS

Carbon nanotubes, aqueous two-phase separation (ATP), aggregate removal, isolation, sorting

ABSTRACT

Isolation and purification of single-walled carbon nanotubes (SWCNTs) is a prerequisite for their implementation in various applications. In this work, we present a fast (~5 minutes), low cost and easily scalable benchtop approach to extract high-quality isolated SWCNTs from bundles and impurities in an aqueous dispersion. The extraction procedure, based on aqueous two-phase separation (ATP), is widely applicable to any SWCNT source (tested up to diameters of 1.7nm), and independent of defect density, purity, diameter, and length. The extracted dispersions show comparable removal of large aggregates, small bundles and impurities to density gradient ultracentrifugation, but without the need for any high end instrumentation. Raman and fluorescence-excitation spectroscopy, single-nanotube fluorescence imaging, atomic force and transmission electron microscopy, and thermo-gravimetric analysis all confirm the high purity of the isolated SWCNTs. By predispersing the SWCNTs without sonication (only gentle stirring) full-length, pristine SWCNTs can be isolated (tested up to 20μm). Hence, this simple ATP method will find immediate application in generating SWCNT materials for all levels of nanotube research and applications, from fundamental studies to high performance devices.

1. Introduction

Single-walled carbon nanotubes (SWCNTs) have been idealized for their intrinsic properties, which depend on their chiral structure [1]. However, purity, heterogeneity, and processability of the as-synthesized materials have limited their widespread implementation in electronics, photonics, and sensor applications. To obtain high purity, isolated SWCNTs in solution, suspension agents have

Address correspondence to Juan G. Duque, jduque@lanl.gov

been used to overcome van der Waals forces between SWCNTs [2-6] combined with strong ultrasonication to break apart bundles [2, 3, 5], inadvertently cutting the SWCNTs in short segments [7].

After predispersion, individual SWCNTs remain in solution along with small carbonaceous and metallic particles and bundles 8, 9], which perturb SWCNT band structure as evidenced by changes in optical signatures [10, 11]. In particular, bundling of SWCNTs can cause red-shifting and broadening in absorption, quenching of fluorescence, and shifting of vibrational Raman signatures [11, 12]. Different techniques have been developed to isolate individual SWCNTs from bundles and other impurities [2-5, 9, 13, 14], with most of these techniques depending on an initial ultracentrifugation (UCF) step followed by a more dedicated technique such as density gradient ultracentrifugation (DGU) [9, 13]. Quantitative techniques, such as rheology and atomic force microscopy (AFM), estimate that after UCF up to 50% of bundles remain [5, 8, 15] and further purification by DGU results in only 5-15% of bundles still present [15, 16].

Both UCF and DGU rely on sedimentation to separate individual SWCNTs from other impurities. UCF is based on sedimentation speed where more dense materials travel more rapidly to the bottom. In contrast, DGU relies upon equilibrium-based sedimentation, where surfactant organization around SWCNTs of different structure and electronic type define the density of dispersed objects that then sediment to a level of equal density [9, 13, 15, 17]. Arnold *et al*. [15] determined with analytical centrifugation that the sedimentation coefficients of bundles and isolated SWCNTs strongly overlap, making their complete separation by UCF unlikely, while DGU can more efficiently remove bundles. Despite the DGU sorting capability, the quality depends on the initial isolation of the predispersion, where higher concentration of bundles will blur the separation lines [9]. All techniques offering increased purity, such as DGU, entail higher costs (including, in particular, use of expensive ultracentrifuges), longer times, more complexities, multiple steps, and lower yields. Thus to streamline commercial advancement, a quick, scalable, low-cost, and high-yield technique is needed. Such a low-cost purification method to remove SWCNT bundles and residual metallic catalyst was proposed with the use of permanent magnets instead of high-end instrumentation [14]. However, since the method relies on differences in magnetic sedimentation of bundles and isolated SWCNTs, compromise must be made on separation time (several hours) versus purity, never able to reach the separation quality of DGU.

Recently, aqueous two-phase separation (ATP) has been introduced as a highly scalable and fast method to separate a wide range of chirality-enriched SWCNT materials [18-22]. In this work we show that the ATP method can also be adjusted to extract isolated SWCNTs and to eliminate production impurities (aggregates, carbonaceous impurities and SWCNT bundles), irrespective of the source materials (HiPco, CoMoCat, Plasma Torch, Arc Discharge and Laser Vaporization). Moreover, our method is extremely fast (~5 min), can simultaneously yield isolation of single chiralities, and is independent of length, achieving DGU-quality isolated individual SWCNTs either from solely stirred (i.e. long, undamaged SWCNTs, lengths up to 20 μm) or sonicated dispersions (i.e. short SWCNTs, <1 μm). The benchtop procedure described does not require expensive and specialized equipment (like an ultracentrifuge), thereby facilitating increased widespread availability of high quality (full-length) isolated SWCNTs.

2. Experimental

SWCNT materials were obtained from various synthesis sources. Table S1 in the Electronic Supplementary Material (ESM) provides an overview of the synthesis source, batch number, and SWCNT diameter range (obtained from UV-vis-NIR absorption). Sodium deoxycholate (DOC, AMRESCO Lot # 0331C075), polyethyleneglycol (PEG, mol.wt. 6000 Da, Alfa Aesar Lot# 10173268), and dextran for 3 different mol. wt. (DX, mol.wt. 70000 Da, TCI Chemicals, Lot # NSBSF-TS; mol.wt. 9000-11000 Da, Sigma Aldrich, Lot # BCBK8656V; and mol.wt. 35000-45000 Da, Sigma Aldrich, Lot # SLBD3835V) were used as received.

SWCNT materials were dispersed in a 1.04%wt/V DOC aqueous solution, either by sonication

(typically 1 hour tip sonication, Sonic Vibra Cell with tip CV18-9909, operated at 8W) or by gentle stirring over a period of 1-3 weeks. For the sonicated suspensions, 1mg/mL raw SWCNT material was dispersed, while for the stirred suspensions a slightly higher starting concentration (1.6mg/mL) was used to achieve better isolation [4].

For separation (unless otherwise stated), these dispersed SWCNTs were added to a PEG:dextran (9%wt/V : 9%wt/V in H_2O, with mol.wt. of dextran 70000Da) stock solution, such that a final DOC concentration of 0.088%wt/V was achieved. A typical separation consisted of adding 400μL of the parent suspension (1.04%wt/V DOC) and 240μL of H_2O to 4080μL of the 9:9%wt/V PEG:dextran solution. The PEG:dextran stock solution was mixed overnight to dissolve the PEG and dextran in water. Immediately after formation of the mixture, the SWCNT/PEG:dextran suspension was benchtop centrifuged for 5 minutes at 6000g to achieve phase separation, and top and bottom fractions were collected manually by a syringe. Unless otherwise stated, all separations were performed at room temperature (22±2°C). Separations for larger diameter SWCNT samples were performed similarly, using D_2O instead of H_2O, which was preferred because of its higher optical transparency in the NIR.

Ultracentrifugation (UCF) and centrifugation (CF) of the pre-dispersed parent suspension, only used for control experiments, were performed on a Thermo-Scientific WX-80 Ultra series ultracentrifuge. For CF, 2 hours at 40000g (17000rpm, TH-641 swing-out rotor) was applied. For UCF comparison, 1 hour at 287000g (40000rpm) was used. For DGU control experiments, a gradient was prepared inside thick-wall polyalomer 2.5mL centrifuge tubes, using iodixanol as gradient medium (Sigma Aldrich, D1556, 60%wt/V). A lower density layer (5% iodixanol and 1%wt/V DOC, 1.4mL), containing the pre-dispersed SWCNTs, was superimposed on a high density layer (27% iodixanol and 1%wt/V DOC, 1mL). The centrifuge tube was tilted (angle ~40°) and rotated around its axis to obtain a quasi-linear gradient. Centrifugation was performed for 20h at 270000g (45000rpm; SW60-Ti swing-out rotor) and the resulting isolated SWCNTs were selected manually by a syringe.

Dialysis of the separated SWCNT phases was performed to remove the polymers after phase separation, using a pressurized Millipore Stirred Ultrafiltration Cell equipped with regenerated cellulose membranes (100kDa). Each phase was filtered until 10% of the volume remained and then 1%wt/V DOC solution was added to dilute the remnants by a factor of 10. This was repeated several times to achieve a minimum dilution of 10^5 for PEG and dextran. Absorption and resonant Raman spectra were acquired to test that this did not result in quantifiable new bundle formation.

For a description of the different experimental techniques, variations of the ATP sorting conditions and data treatments we refer to the ESM.

3. Results and Discussion

In ATP separations, two water-soluble but immiscible polymers, e.g. PEG and dextran, are mixed together after which they spontaneously form two phases with different hydrophobicity [23]. The resulting top phase, i.e. PEG-rich phase, is less hydrophilic than the dextran-rich bottom phase. Tuning the surfactant structure around the SWCNT surface results in differences in relative hydrophobicities of various SWCNT species [20]. Different chiralities thus separate into the different phases. With our current understanding of the separation mechanism [20], we sought to develop a technique to separate isolated SWCNTs from bundles and other production impurities.

We started from a stock dispersion of PEG and dextran, both with 9% wt/V concentration, and added different amounts of a 1.04%wt/V DOC - SWCNT parent suspension to this stock solution (with corresponding H_2O addition to have similar dilution factors), and subsequently induced the phase-separation by benchtop centrifugation for 5 minutes at 6000g. Figure 1a presents the absorption spectra of a sonicated parent HiPco-SWCNT dispersion (in black), and spectra of top (in blue), bottom (in red), and interface (in green) after phase separation with a final DOC concentration of 0.088% wt/V. Unless otherwise stated, for proper comparison, absorption spectra of top, bottom, and interface are rescaled, according to their specific volumetric

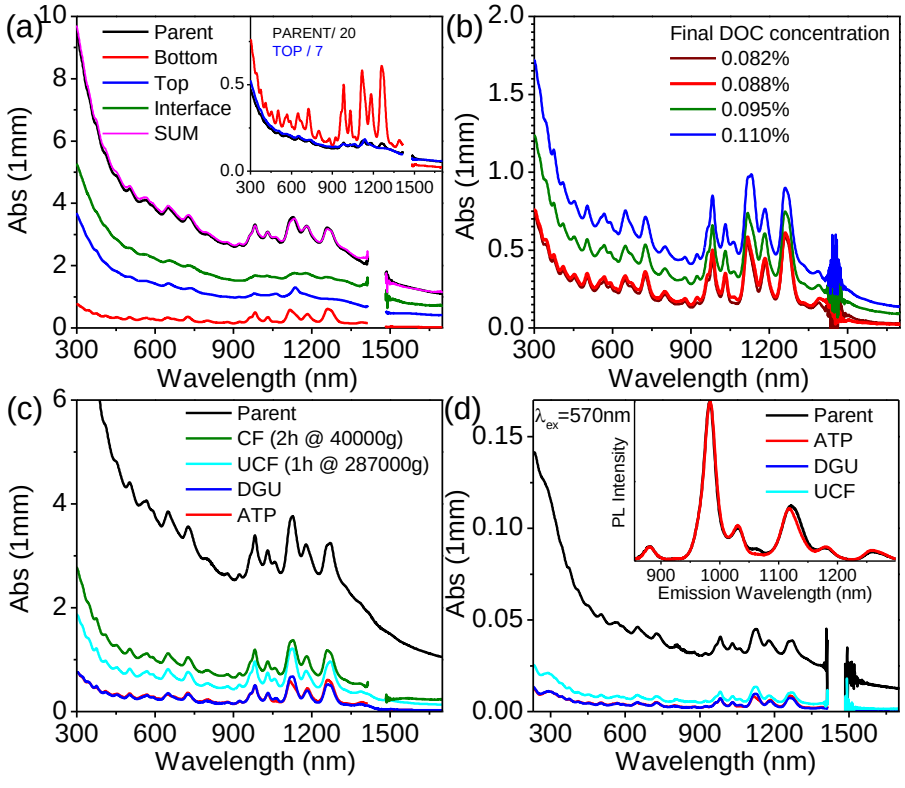

Figure 1: Absorption spectra of ATP separated HiPco 195.2 SWCNTs. (a) Absorption spectra of the parent HiPco 195.2 suspension (black), bottom (red), top (blue) and interface (green) for an ATP separation with a final DOC concentration of 0.088%wt/V. The bottom (1180 µL) and top (3540 µL) absorption spectra were rescaled according to their volumetric dilution (see ESM), while the interface (unknown volume) was rescaled so that SUM=bottom + top + interface (shown in magenta) matches the absorption signal of the parent suspension. The inset shows an expanded absorption spectrum of the ATP bottom separated phase, in comparison to a rescaled absorption spectrum of the top (divided by 7) and parent (divided by 20) suspensions, revealing a much higher SWCNT - to - background ratio in the absorption spectra of the bottom phase. Samples were diluted if necessary for the absorption measurements (Optical Density < 3) and afterwards rescaled according to this dilution factor. (b) Absorption spectra of the ATP bottom phases for different final DOC concentrations, showing that 0.088%wt/V ideally removes the impurity-related background. (c) Comparison of the absorption spectra of the parent HiPco 195.2 SWCNT dispersion (black) and bundle-removal by CF (2h @ 40.000g, green), UCF (1h @ 287.000g, cyan), DGU (20h@270.000g, blue) and ATP (5 min @ 6.000g, red). Parent, CF and UCF spectra are presented as measured, ATP was corrected for its volumetric dilution and DGU was rescaled on the intensity of the excitonic transitions of the ATP separation, showing that the background - to - SWCNT absorption is identical for ATP and DGU, while in CF and UCF a significant fraction of the background remains present. (d) Absorption spectra of the ATP separated (red), DGU (blue), UCF (cyan) and parent SWCNT dispersion (black), diluted and rescaled to obtain a normalized PL intensity after excitation at 570nm (see inset for comparison of parent and ATP separated PL, DGU and UCF yield similar PL spectra but are omitted for clarity). All absorption data are cut around 1400nm due to strong H_2O absorbance in this region.

dilution after phase separation (for details see ESM section S2.a), as previously reported [20]. After proper rescaling, the sum of bottom, top, and interface (in magenta) matches the absorption signatures of the parent suspension.

The absorption spectrum of the bottom phase (red curve in Fig. 1a) shows sharp excitonic transitions of all isolated SWCNT chiralities, but with a strong reduction in background (in comparison with the parent suspension). In contrast, the more hydrophobic top phase (and the interface) contains a strong absorption 1/λ-like scattering background (arising from all scatterers, including larger aggregates) and highly broadened excitonic transitions (arising from small aggregates: SWCNT-SWCNT interactions typically broaden and red-shift SWCNT transitions [11, 12]), suggesting a

significant difference in solution content of both phases. The strong background removal is also visualized in the inset of Fig. 1a, where spectra of parent and top suspensions are rescaled on this background, showing much smaller contributions of resonant SWCNT absorption (due to much higher relative contribution of background in those samples). We hypothesize that such significant spectroscopic differences are due to the removal of aggregates, carbonaceous impurities, and small SWCNT bundles.

Figure 1b presents rescaled absorption spectra of the bottom phases after varying the final DOC concentration for the separation, which was achieved by stepwise varying the amounts of added H_2O and parent suspension (without changing the total dilution factor). The scaled spectra demonstrate that a slightly higher DOC concentration (compared to the one used in Fig. 1a, from 0.088 to 0.110%) results in the appearance of additional background absorption, while hardly any relative intensity increase for the excitonic SWCNT absorbance can be observed. A slightly lower DOC concentration (0.082%) than 0.088%, provides no further removal of background signal, but results in partial removal and aggregation of specific chiralities (e.g. the (10,2) chirality with E_{11}=1062nm). A final DOC concentration of 0.088%wt/V was found to be ideal for the removal of the large scattering background in the absorption spectra, without removing specific chiralities from the bottom phase.

Figure 1c compares this ATP separation (bottom phase) with separation of isolated SWCNTs starting from the same parent suspension via normal centrifugation (CF; 2h at 40000g), UCF (1h at 2870000g), known to retain 15-50% bundles of smaller than 4nm in diameter [5, 8, 15], and DGU (20h at 270000g), known to retain 5-15% of bundles [8, 9, 15]. When comparing peak-to-valley ratios for the (6,5) chirality (i.e. peak = 982nm, valley = 901nm) for the different separations, we obtain 1.34 for the parent suspension, 1.8 for CF, 2.24 for UCF, 3.35 for DGU, and 3.35 for ATP, thus showing significant background reduction from the parent dispersion for all methods, but with ATP and DGU achieving the greatest reduction. Most importantly, the ratios clearly show identical results for DGU and ATP, indicating an equivalent removal of bundles and other impurities by ATP as by DGU.

A further measure of the improved isolation of the ATP-extracted SWCNTs comes from an increased sample PL intensity, which is highly sensitive to environmental effects and dispersion quality [24]. For accurate comparison, ATP separated bottom fractions and DGU samples were first dialyzed into 1 %wt/V DOC to remove PEG and dextran. All samples were diluted to eliminate self-absorption effects (optical density (OD) < 0.05 in a 1 mm cell) and such that their (6,5) PL intensity exciting at 570 nm is identical (inset Fig. 1d inset and Fig. S1 in ESM). Since the PL mainly originates from isolated SWCNTs and not non-fluorescent absorbing impurities, a much higher concentration, overall absorption, of the parent dispersion is needed to achieve the same PL intensity as the purified dispersions. Moreover, the slightly

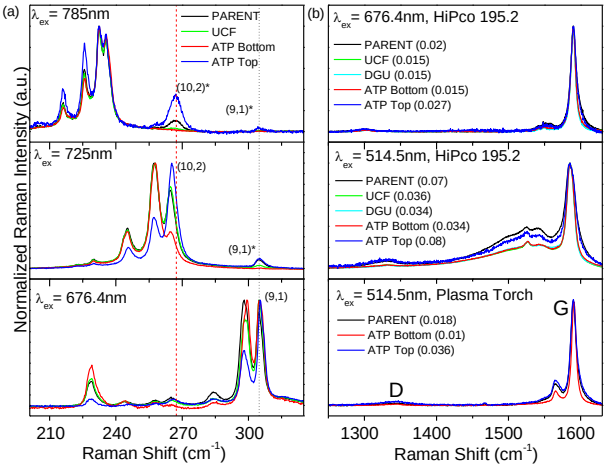

Figure 2: Resonant Raman spectroscopy (RRS) of the ATP separated samples. (a) RRS spectra of the RBM-region for HiPco 195.2 excited at 3 different wavelengths, showing the radial breathing modes of different chiralities, e.g. (9,7), (10,5), (11,3) and (12,1) SWCNTs in resonance at 785nm (left to right). The RBM of the (10,2) SWCNT, i.e. 266cm^{-1} (indicated by the red dashed line), is clearly resonant at 725nm, while at 785nm excitation this RBM is only resonant when bundles are present [12]. Similarly the RBM of the (9,1) SWCNT, indicated by the black dashed line at 310cm^{-1} is resonant at 676.4nm, while at 725nm this RBM is only resonant when bundles are present. Bundles are thus mainly present in the top phase and at the interface after bundle-extraction. (b) RRS spectra of the D- and G-bands excited at 514.5nm and 676.4nm, for the HiPco 195.2 and Plasma Torch SWCNTs. D/G ratios are presented in parenthesis. The ATP bottom fraction has narrower G-band line width and a lower D/G ratio indicating the higher purity of this sample in comparison with the parent suspension.

greater absorption of the UCF dispersion, relative to ATP and DGU, corroborates the presence of more impurities and bundles contributing to the overall absorption. Raman spectroscopy, Atomic Force Microscopy (AFM), Transmission Electron Microscopy (TEM), and Thermogravimetric Analysis (TGA) were used to further evaluate the relative purity of the ATP extracted SWCNTs. SWCNT isolation is confirmed by Raman spectra (Fig. 2a) obtained at 785 nm excitation, where bundling shifts the resonance conditions for the (10,2)-SWCNT (d= 0.884 nm) from 735 nm to 785 nm, making its radial breathing mode at 266cm^{-1} more prominent as bundle content increases [12]. Given that (10,2)-SWCNTs might not be present in all source materials, we searched for a new SWCNT family to probe bundle formation. The (9,1) SWCNT (d= 0.757 nm) normally resonant at 680 nm becomes resonant at 725 nm when bundled and serves as an alternative probe for bundle identification. Thus, the presence of the Raman bundling peaks reveals that unlike either ATP or DGU, the absorption spectra of the dispersions obtained by CF and UCF maintain a significant background due to the presence of bundles (Fig. 2). The Raman D/G ratios at different excitation wavelengths (Fig. 2b) shows that the G-band line-width and D/G ratios reduce similarly for ATP and DGU (relative to the parent and UCF samples), indicating highly isolated samples after ATP separation [26, 27].

AFM (Fig. 3a) corroborates minimal bundles in the bottom phase, and indicates that most bundles remain in the top and interfacial layers. Statistical analysis of the AFM data (Fig. 3b) reveals at least 90% of the SWCNT present in the bottom phase are well isolated or not bundled, some of which were created during AFM sample preparation. TGA confirms a decrease in catalyst concentration after ATP extraction, corroborated by TEM (see Fig. S2), from 26.4% in the starting raw sample to 12.6% in the bottom phase (similar to UCF and magnetic purifications [14], Fig. S3). Since ATP and DGU are equilibrium-based separations, unlike UCF or magnetic purification that are rate-based, a greater isolation from impurities can be achieved without sacrificing yield.

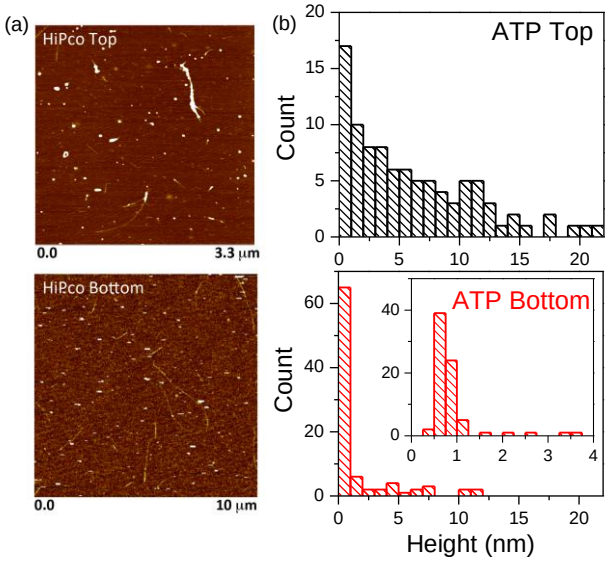

Figure 3: AFM analysis of the separated fractions. (a) Representative AFM image of the top and bottom phase after bundle extraction for the parent HiPco 195.2 dispersion, showing many more impurities and bundles in the top phase and (b) height statistics of the AFM images, revealing 90% of isolated SWCNTs in the bottom phase (note that HiPco diameters range from ~0.54-1.2nm[25] and that AFM sample deposition might cause a small degree of bundling). The inset zooms in on the relevant region for the bottom phase.

The mechanism of ATP separation is directly dictated by its constituent hydrophobicities [23], not intrinsic SWCNT hydrophobicity [8]. As such, parameters that are not directly related to the hydrophobicity of the SWCNT/micelle system, all yield similar SWCNT extractions (Fig. 4a-b and Fig. S4). For example, no change in isolation quality is apparent when increasing the sonication time (Fig. 4a) or the SWCNT starting concentration (Fig. S4 in ESM), which only result in a higher overall concentration of isolated SWCNTs. As well, an additional centrifugation step prior to the ATP separation to partially remove bundles only slightly reduces the separation yield (Fig. 4b). For parameters that affect the relative hydrophobicity of the two phases however, a different SWCNT isolation is achieved (Fig. 4c-d, Fig. S5 and S6 in ESM). However, the versatility of the method allows one to compensate these small changes with small changes of the DOC concentration used for the separation; decreasing DOC concentration until optimal, increases the number of isolated SWCNTs in the bottom phase, while increasing DOC concentrations until optimal,

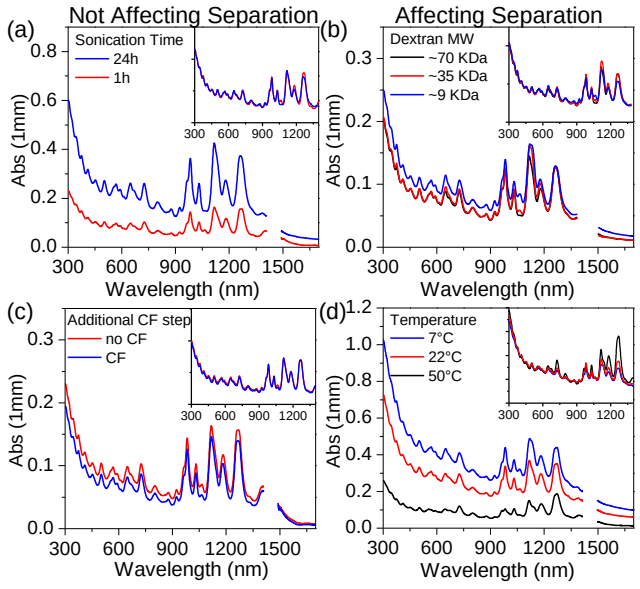

Figure 4: Parameters that affect and those that do not affect the separation. *Not Affecting separation*: (a) Variation of sonication time: As measured absorption spectra of the ATP bottom phases for a HiPco 195.2 parent suspension prepared with either 1 or 24 hours of sonication. After rescaling (inset), no significant change in the chirality distribution nor in the ratio of background to SWCNT signals is found. (b) As measured absorption spectra of the ATP bottom phase for two different parent suspensions, with and without a pre-centrifugation step. Only a slight overall decrease of the signals, no change in ratio background versus SWCNT signals (see inset for rescaled absorption spectra). *Affecting Separation*: (c) Volumetric diluted absorption spectra of the ATP-separated bottom phases for different dextran MW, with the inset presenting the rescaled absorption spectra. (d) As measured absorption spectra of the ATP separated bottom phase for different separation temperatures. At high temperature, individualized SWCNTs move to the top phase, while at low temperature background increases due to more bundles and impurities separating in the bottom phase. All separations were performed using a fixed DOC concentration of 0.088%wt/V.

removes bundles from the bottom phase (Fig. 1b).

intrinsic SWCNT hydrophobicity [8]. As such, parameters that are not directly related to the hydrophobicity of the SWCNT/micelle system, all yield similar SWCNT extractions (Fig. 4a-b and Fig. S4). For example, no change in isolation quality is apparent when increasing the sonication time (Fig. 4a) or the SWCNT starting concentration (Fig. S4 in ESM), which only result in a higher overall concentration of isolated SWCNTs. As well, an additional centrifugation step prior to the ATP separation to partially remove bundles only slightly reduces the separation yield (Fig. 4b). For parameters that affect the relative hydrophobicity of the two phases however, a different SWCNT isolation is achieved (Fig. 4c-d, Fig. S5 and S6 in ESM). However, the versatility of the method allows one to compensate these small changes with small changes of the DOC concentration used for the separation; decreasing DOC concentration until optimal, increases the number of isolated SWCNTs in the bottom phase, while increasing DOC concentrations until optimal, removes bundles from the bottom phase (Fig. 1b).

Albertsson *et al*. [23] showed that by lowering the molecular weight of dextran, the phase separation and thus the redistribution of the particles across the two phases is altered with more particles separating into the bottom phase. Likewise, in our separation, lower dextran MW results in a small fraction of bundles reaching the bottom phase (mol. wt. 9000Da), which can be corrected by decreasing the DOC concentration (Fig. 4c and Fig. S5 in ESM), resulting in an identical quality and distribution of isolated SWCNTs. Such control permits the use of lower molecular weight and low cost industrial grade dextran, which would be beneficial for ease of dialysis after separation (to remove the polymers from the separated fractions) and to reduce the separation cots. Similar to other separation techniques [28], ATP separations are sensitive to temperature [19], due to its significant effect on the specific surfactant structure [29], thereby altering the hydrophobicity. Typically, lower temperature results in more bundles in the bottom phase, while higher temperature results in less isolated SWCNTs in the bottom phase, but both can be corrected by altering the DOC concentration (Fig. 4d).

We furthermore prepared SWCNT dispersions and performed a similar separation using sodium dodecylsulfate (SDS) and sodium cholate (SC) as the dispersing agent in the same PEG/dextran stock solution (Fig. S6). SDS is unable to extract only individualized SWCNTs, with bundles and most isolated SWCNTs separating into the same (top) phase; the small amount that does remain in the bottom phase contains bundles. With SC, individual SWCNTs can be isolated; however, a higher

concentration of surfactant is needed than with DOC, since at lower concentrations, the resulting distribution of isolated SWCNTs is skewed toward small-diameter SWCNTs. Briefly, the differences in surfactant behaviors are due to the dynamic nature of their wrapping configurations, which can be linked to their molecular structure as previously discussed in detail [20].

For a particular separation technique to be of high impact, it is crucial to demonstrate that it is widely applicable for a variety of SWCNT source materials. Different SWCNT production methods (Table S1 in ESM), including less expensive sources, offer variable diameter distributions, production related defect densities, and SWCNT content (e.g. Arc-discharge synthesis typically yields <40% SWCNT content [27]). Importantly, the dominant physical parameters of the SWCNTs (defect density, diameter, and length) should not affect the constituent hydrophobicities and thus the quality of isolation.

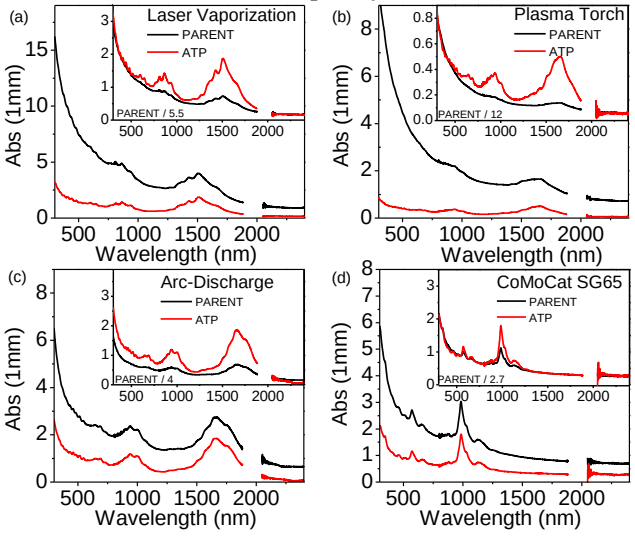

Figure 5: ATP isolation of SWCNTs from different sources (parent suspensions prepared in D_2O for optical transparency in the NIR). Absorption spectra of the parent (black) and resulting ATP bottom fractions (red) for (a) Laser vaporization SWCNTs; (b) Plasma Torch (Raymor) SWCNTs; (c) Arc-discharge SWCNTs and (d) CoMoCat SG65 SWCNTs. Absorption spectra are presented for 1mm path length, and ATP bottom fractions are rescaled according to the volumetric dilution. The insets of each panel present a zoomed-in absorption of the ATP-sorted bottom fractions in comparison with a rescaled absorption of the parent suspension (long-wavelengths normalization). The scaling factors for the parent suspension are also given. Data are cut around 2000nm, due to small H_2O absorption in the D_2O-sorted samples.

Figure 5 shows the absorption spectra of samples, before and after ATP separation, of various SWCNT source materials used across the vast SWCNT literature.

ATP successfully removes impurities from all sources exhibiting the same background reduction shown in HiPco dispersions. To better assess the changes in spectra, we scaled the absorption of the parent dispersions such that both spectra coincide at high wavelengths (i.e. rescaling on the non-resonant carbon absorbance, insets of Fig. 5a-d). Spectral resolution for all ATP isolated SWCNT samples exceed that of the parent suspensions, revealing the excitonic transitions that are overshadowed in the parent samples by strong backgrounds attributable to the presence of impurities and bundles. AFM images of the top and bottom phase of Plasma Torch CNTs (Fig. S7 in ESM), TEM (Fig. S8 in ESM) and RRS spectra (Fig. 2b) confirm mostly isolated SWCNTs are extracted to the bottom phase while carbonaceous impurities and bundles separate into the top phase.

To better evaluate the quality of SWCNT isolation from a low cost source, we compared spectra from parent, centrifuged, and ATP dispersions of Plasma Torch SWCNTs from Raymor Technologies. A relative PL efficiency is presented in Fig. 6a, where PL measurements were scaled by respective sample absorbance at the 800nm excitation wavelength. Upon centrifugation, SWCNT fluorescence increases by a factor of two, whereas ATP separated dispersions achieve an order of magnitude greater PL for a given sample absorption (absorption at 800nm). The quality of the isolated Plasma Torch SWCNTs is highlighted by the PLE map identifying emitting SWCNTs with diameters from ~1-1.5nm (Fig. 6b).

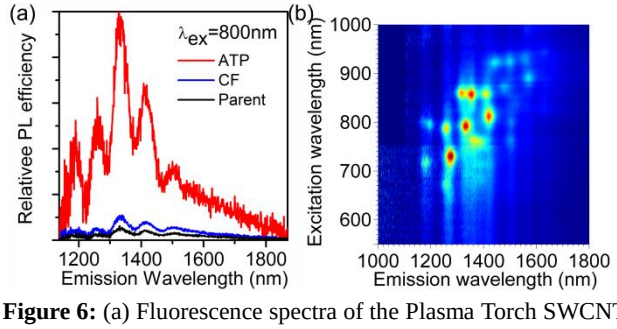

Figure 6: (a) Fluorescence spectra of the Plasma Torch SWCNTs from Raymor parent (black), centrifuged (blue) and ATP sorted bottom phase (red). PL intensity is scaled by the absorbance at

the excitation wavelength (800nm) to obtain a relative dispersion PL efficiency. (b) 2D NIR PLE map of Plasma Torch ATP separated bottom fraction, showing excitonic transitions of SWCNTs in the 1-1.5nm diameter range. The PLE spectrum was calibrated for excitation light intensity and detector sensitivity.

Likewise, the bottom fractions in all tested source materials exhibit well-resolved PL peaks indicative of high-quality SWCNT isolation (Fig. S9). Recent work has furthermore shown that the PL can even be further enhanced with plasmonic colloidal suspensions [30]. Thus, separation of SWCNTs from various sources offers a large range of isolated diameters, which are instrumental for enabling a broad range of SWCNT applications. For instance, while SWCNT photovoltaics show better performance with small diameter SWCNTs [31], transistors require large diameters [32, 33], and biological imaging needs diameters (i.e. band-gap) tuned [2, 34, 35] to avoid absorption by water, tissue, etc..

Besides the applicability of the method for a wide range of source materials, the scalability and repeatability of the method is extremely important for a new purification method to meet application needs. We therefore performed separations on a 0.472 mL, a 4.72 mL and a 47.2 mL scale, thus generating bottom fractions from 90 μL to 9 mL in the same time frame. All separations achieve identical separations irrespective of 2 orders of magnitude change in volume scale (Figure 7).

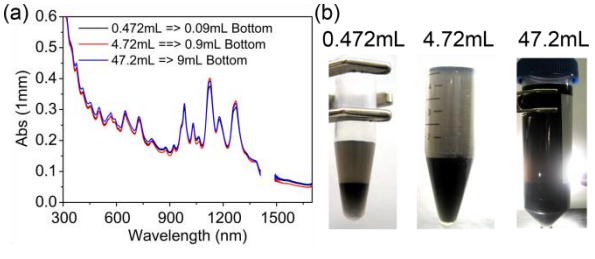

Figure 7: Scalability of the ATP separation: (a) As-measured absorption spectra of the ATP bottom fractions after separating in 3 different volumes, resulting in 90 μL, 900 μL and 9mL of bottom fraction. (b) Photographs of the resulting phase-separations.

Finally, large-scale isolation of pristine, full-length SWCNTs has remained elusive in the SWCNT community, as most separation methods demand intense sonication [2, 3, 5], which reduces the original aspect ratio (full-length). Various SWCNT applications, such as conductive/strong fibers [36], thin-film transistors [32], strain sensors [37] and conductive transparent films [38, 39], as well as experimental studies [40] have stressed the importance of long, pristine SWCNTs to enhance mechanical strength, electrical/thermal conductivity

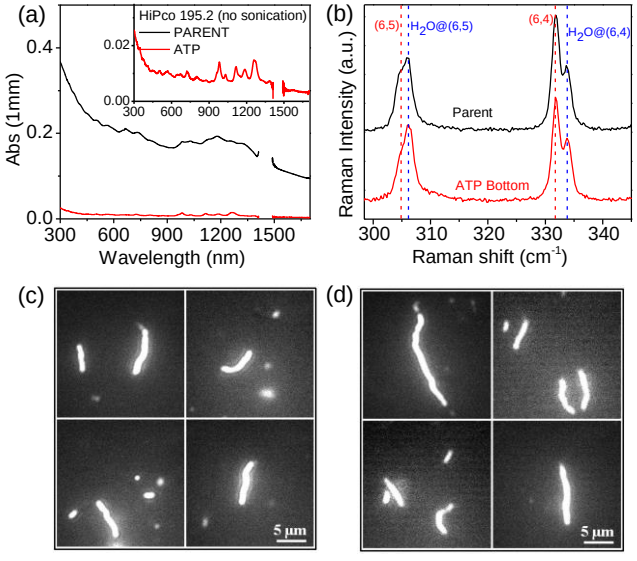

Figure 8: ATP separation of stirred SWCNT samples (no sonication; long SWCNTs). (a) Absorption spectra of the parent (black) and ATP bundle-extracted bottom phase (as according to its volumetric dilution) (red) for HiPco 195.2 SWCNT dispersion, prepared without sonication. The inset presents an expanded absorption spectrum of the ATP bottom phase. (b) RRS spectra excited at 570nm for the starting HiPco 195.2 stirred parent solution, and the ATP sorted bottom phase. Red and blue dashed lines indicate positions of empty and water-filled (H2O@CNT) SWCNTs, respectively. Ratios between empty and water-filled RBM intensities remain constant after separation. (c-d) representative set of PL images (excitation 570 nm, CCD detection) of the parent (c) and ATP bottom (d) phase after bundle-extraction, clearly showing both short and long SWCNTs are separated in a similar way.

and optical quality. Full-length SWCNTs not only have higher aspect ratios, but are also less defective and display improved optical properties [41, 42]. Only a few studies have reported isolation of long SWCNTs by DGU [42, 43], but at the cost of simplicity, time and scalability. To generate long, pristine SWCNT dispersions using our ATP-technique, the SWCNT-surfactant mixture is gently stirred over a period of 1-3 weeks [4], typically

resulting in a mixture of closed ('pristine') and opened ('cut') SWCNTs with few defects [7, 25, 41, 42]. Figure 8a (and Fig. S10 in ESM) demonstrates that ATP can be used to successfully extract isolated SWCNTs from these dispersions (red trace), resulting in a significant reduction of the background absorption and sharp excitonic transitions, which are not resolved in the parent dispersion (black trace). The significant changes in the background and excitonic linewidth are directly associated with the lower SWCNT isolation obtained by simple stirring, however by stirring a higher SWCNT concentration, very similar optical density of the resulting bottom fractions can be obtained (comparing insets of Fig. 1b with Fig. 8a). PL images (Figure 8c-d) of the isolated SWCNTs and parent dispersion show that SWCNTs up to 20 μm in length remain after ATP separation. AFM measurements (Fig. S11) confirm that mostly isolated long SWCNTs are present in the bottom phase, while the majority of bundles and other impurities remain in the top phase. A further measure of the gentleness of this extraction technique can also be demonstrated by high resolution RRS, which allows resolving the presence of closed (empty, pristine) and opened (water-filled) SWCNTs, since the water-filled SWCNTs have slightly blue-shifted RBM vibrations [7, 25, 41, 42]. Figure 8b presents such Raman spectra excited at 570nm for the stirred HiPco parent solution and the ATP sorted bottom phase, clearly indicating that a significant fraction of the SWCNTs are closed since no sonication was applied, and that the ratio of closed-to-opened SWCNTs remains the same after separation. These results demonstrate that ATP multi-chiral separation can be achieved, independent of the length and average diameter of SWCNTs.

Similarly, we have applied our previous single-chirality (6,5) separation approach [20] to these stirred SWCNT samples, while also avoiding a prior UCF step, to achieve a fast single-chirality separation of full-length SWCNTs. A similar distribution of SWCNT chiralities is achieved with minimal background in absorption spectra for both sonicated (1h) and stirred samples (Figure 9a). Notably, sonication increases the overall concentration of isolated SWCNTs in the parent solution and thus a greater amount of (6,5)-SWCNT enrichment after separation, though at the cost of shortening. Figures 9b and 9c show single-SWCNT PL images after ATP (6,5) enrichment of long and short SWCNTs, respectively, revealing that even one hour of sonication generates samples with SWCNTs no longer than 1μm while stirring maintains full-length SWCNTs (up to 20μm in the studied samples). Moreover, this confirms that the chirality separation is determined by the specific surfactant composition covering the SWCNTs, independent of their length.

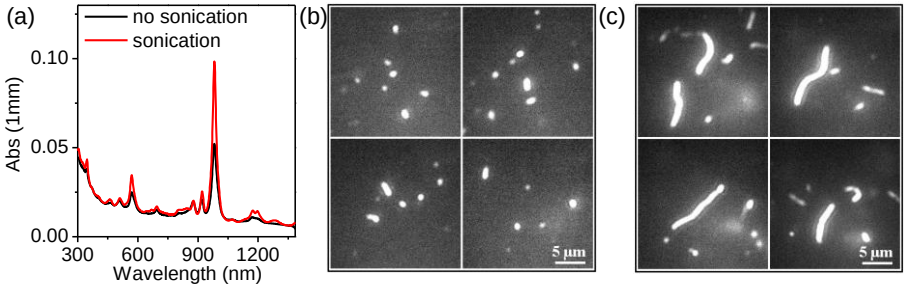

Figure 9: Single-chirality (6,5) ATP separation [20] for short and long SWCNTs. (a) As-measured absorption spectra of (6,5) sorted bottom phases for stirred (no sonication, black) and tip-sonicated (1 hour, red) HiPco 195.2 SWCNT dispersion after ATP isolation. (b-Cc) Representative set of PL images (excitation 570 nm, CCD detection) of the sonicated (b) and non-sonicated (c) (6,5) fractions showing the influence of sonication on the length distribution in the samples.

Availability of long pristine SWCNTs should find immediate applications in conductive transparent thin-films and aligned arrays of long SWCNTs for technologies such as photovoltaics, video displays, transistors, conductive/strong fibers, and solid-state lighting. The performance of such devices should benefit tremendously from very long SWCNTs, since longer SWCNTs lower the percolation threshold and can enhance SWCNT alignment over long distances, which in turn lowers the resistance of thin-films, increases the strength and conductivity of fibers, and increases carrier mobility, on-currents, and on/off

ratios of transistors [39, 44].

4. Conclusions.

Here we report multi-chirality isolation of individual SWCNTs through a simple ATP technique. Our technique achieves DGU quality dispersions in a timely, inexpensive, and highly accessible manner attaining low background absorption and sharp excitonic transitions, due to the removal of starting impurities and bundles. With such purified samples we were able to identify a new resonance condition (725 nm) where the (9,1) SWCNT-family comes into resonance as a result of bundling serving as an alternative standard (to the typically utilized (10,2) standard) to probe bundle presence.

Remarkably, this technique extracts high-quality isolated SWCNT dispersions from any SWCNT source, irrespective of purity, diameters (tested up to 1.6 nm), opened/closed ratio, and length (tested up to 20 μm), substantiating our claim that the nature of the nanotubes does not directly affect the hydrophobicity of the system and thus the quality of isolation. Moreover, controlling the constituents affecting hydrophobicity enables tunability toward desired multi- and single-chirality isolations. Such control enables the use of cheap SWCNTs (e.g. Plasma Torch (Raymor)) to achieve inexpensive high-quality isolated SWCNT dispersion. Future studies will explore variation of our techniques toward isolation of larger diameter SWCNT, few-walled carbon nanotubes, open/closed separation, and metal/semiconductor separation and development of a procedure to accurately measure the overall yield of all separations.

We anticipate that as observed in the surge of graphene research that followed the introduction of solution phase processing [45], our ability to create high-quality suspensions via high-throughput, inexpensive, and gentle methods from low-cost materials without expensive instruments (replacing UCF by bench-top centrifugation and potentially without any sonication) will kindle new SWCNT research in multidisciplinary fields, promoting innovation in fundamental research and high-performance devices. Furthermore, our approach will accelerate the incorporation of isolated long SWCNTs from low-cost sources into rapidly emerging commercial applications such as material reinforcement, sensors, field-effect transistors, and photovoltaics where large quantities of full-length CNTs are required in a cost effective manner.

Acknowledgements

We thank Kevin Henderson for access to TGA and Wim Wenseleers for helpful discussions. This work was supported by the LANL-LDRD program and was performed in part at the Center for Integrated Nanotechnologies, a U.S. Department of Energy, Office of Basic Energy Sciences user facility. S.C. gratefully acknowledges the financial support from the Fund for Scientific research Flanders, Belgium (FWO-Vlaanderen) for providing a postdoctoral fellowship and a mobility grant for visiting the Los Alamos National Laboratory. A.N.G.P.V. gratefully acknowledges support from the LANL Director's Postdoctoral Fellowship. LV SWCNT synthesis was performed at NREL, and was supported by the Solar Photochemistry Program, Division of Chemical Sciences, Geosciences, and Biosciences, Office of Basic Energy Sciences, U.S. Department of Energy (DOE), Grant DE-AC36-08GO28308..

Electronic Supplementary Material: Supplementary material (description of materials, methods used for the spectroscopic and image characterization, and supporting figures as referred to in the manuscript) is available in the online version of this article at http://dx.doi.org/10.1007/s12274-***-****-*.

References

[1] Jorio, A.; Dresselhaus, G.; Dresselhaus, M. S. *Carbon Nanotubes: Advanced Topics in Synthesis, Structure, Properties and Applications*; Springer-Verlag: Berlin, 2008.

[2] O'Connell, M. J.; Bachilo, S. M.; Huffman, C. B.; Moore, V. C.; Strano, M. S.; Hároz, E. H.; Rialon, K. L.; Boul, P. J.; Noon, W. H.; Kittrell, C.; *et al*. Band gap fluorescence from individual single-walled carbon nanotubes. *Science* **2002**, *297*, 593-596.

[3] Islam, M. F.; Rojas, E.; Bergey, D. M.;

Johnson, A. T.; Yodh, A. G. High weight fraction surfactant solubilization of single-wall carbon nanotubes in water. *Nano Lett.* **2003**, *3*, 269-273.

[4] Wenseleers, W.; Vlasov, I.I.; Goovaerts, E.; Obraztsova, E. D.; Lobach, A. S.; Bouwen, A. Efficient isolation and solubilization of pristine single-walled nanotubes in bile salt micelles. *Adv. Funct. Mater.* **2004**, *14*, 1105-1112.

[5] Cathcart, H.; Quinn, S.; Nicolosi, V.; Kelly, J. M.; Blau, W. J.; Coleman, J. N. Spontaneous debundling of single-walled carbon nanotubes in DNA-Based dispersions. *J. Phys. Chem. C* **2006**, *111*, 66-74.

[6] Gerstel, P.; Klumpp, S.; Hennrich, F.; Altintas, O.; Eaton, T. R.; Mayor, M.; Barner-Kowollik, C.; Kappes, M. M. Selective dispersion of single-walled carbon nanotubes via easily accessible conjugated click polymers. *Polym. Chem.* **2012**, *3*, 1966-1970.

[7] Wenseleers, W.; Cambré, S.; Culin, J.; Bouwen, A.; Goovaerts, E. Effect of water filling on the electronic and vibrational resonances of carbon nanotubes: characterizing tube opening by Raman spectroscopy. *Adv. Mater.* **2007**, *19*, 2274-2278.

[8] Parra-Vasquez, A. N. G.; Duque, J. G.; Green, M. J.; Pasquali, M. Assessment of length and bundle distribution of dilute single-walled carbon nanotubes by viscosity measurements. *AIChE Journal* **2014**, *60*, 1499-1508.

[9] Bonaccorso, F.; Hasan, T.; Tan, P. H.; Sciascia, C.; Privitera, G.; Di Marco, G.; Gucciardi, P. G.; Ferrari, A. C. Density gradient ultracentrifugation of nanotubes: Interplay of bundling and surfactants encapsulation. *J. Phys. Chem. C* **2010**, *114*, 17267-17285.

[10] Arnold, M. S.; Stupp, S. I.; Hersam, M. C. Enrichment of single-walled carbon nanotubes by diameter in density gradients. *Nano Lett.* **2005**, *5*, 713-718.

[11] Tabakman, S. M.; Welsher, K.; Hong, G.; Dai, H. Optical properties of single-walled carbon nanotubes separated in a density gradient: Length, bundling, and aromatic stacking effects. *J. Phys. Chem. C* **2010**, *114*, 19569-19575.

[12] O'Connell, M. J.; Sivaram, S.; Doorn, S. K. Near-Infrared resonance Raman excitation profile studies of single-walled carbon nanotube intertube interactions: A direct comparison of bundled and individually dispersed HiPco nanotubes. *Phys. Rev. B* **2004**, *69*, 235415.

[13] Arnold, M. S.; Green, A. A.; Hulvat, J. F.; Stupp, S. I.; Hersam, M. C. Sorting carbon nanotubes by electronic structure using density differentiation. *Nature Nanotechnol.* **2006**, *1*, 60-65.

[14] Ghosh, S.; Bachilo, S. M.; Weisman, R. B. Removing aggregates from single-walled carbon nanotube samples by magnetic purification. *J. Phys. Chem. C* **2014**, *118*, 4489-4494.

[15] Arnold, M. S.; Suntivich, J.; Stupp, S. I.; Hersam, M. C. Hydrodynamic characterization of surfactant encapsulated carbon nanotubes using an analytical ultracentrifuge. *ACS Nano* **2008**, *2*, 2291-2300.

[16] Naumov, A. V.; Kuznetsov, O. A.; Harutyunyan, A. R.; Green, A. A.; Hersam, M. C.; Resasco, D. E.; Nikolaev, P. N.; Weisman, R. B. Quantifying the semiconducting fraction in single-walled carbon nanotube samples through comparative atomic force and photoluminescence microscopies. *Nano Lett.* **2009**, *9*, 3203-3208.

[17] Fagan, J. A.; Zheng, M.; Rastogi, V.;

Simpson, J. R.; Khripin, C. Y.; Batista, C. A. S.; Walker, A. R. H. Analyzing surfactant structures on length and chirality resolved (6,5) single-wall carbon nanotubes by Analytical Ultracentrifugation. *ACS Nano* **2013**, *7*, 3373-3387.

[18] Khripin, C. Y.; Fagan, J. A.; Zheng, M. Spontaneous partition of carbon nanotubes in polymer-modified aqueous phases. *J. Am. Chem. Soc.* **2013**, *135*, 6822-6825.

[19] Fagan, J. A.; Khripin, C. Y.; Silvera Batista, C. A.; Simpson, J. R.; Hároz, E. H.; Hight Walker, A. R.; Zheng, M. Isolation of specfic small diameter single-wall carbon nanotube species via aqueous two-phase extraction. *Adv. Mater.* **2014**, *26*, 2800-2804.

[20] Subbaiyan, N. K.; Cambré, S.; Parra-Vasquez, A. N. G.; Hàroz, E. H.; Doorn, S. K.; Duque, J. G. Role of surfactants and salt in aqueous two-phase separation of carbon nanotubes toward simple chirality isolation. *ACS Nano* **2014**, *8*, 1619-1628.

[21] Zhang, M.; Khripin, C. Y.; Fagan, J. A.; McPhie, P.; Ito, Y.; Zheng, M. Single-step total fractionation of single-wall carbon nanotubes by countercurrent chromatography. *Anal. Chem.* **2014**, *86*, 3980-3984.

[22] Ao, G.; Khripin, C. Y.; Zheng, M. DNA-controlled partition of carbon nanotubes in polymer aqueous two-phase systems. *J. Am. Chem. Soc.* **2014**, *136*, 10383-10392.

[23] Albertsson, P.-A. *Partition of Cell Particles and Macromolecules: Separation and Purification of Biomolecules, Cell Organelles, Membranes and Cells in Aqueous Polymer Two Phase Systems and Their Use in Biochemical Analysis and Biotechnology.*; John Wiley and Sons, 1986.

[24] Duque, J. G.; Pasquali, M.; Cognet, L.; Lounis, B. Environmental and synthesis-dependent luminescence properties of individual single-walled carbon nanotubes. *ACS Nano* **2009**, *3*, 2153-2156.

[25] Cambré, S.; Schoeters, B.; Luyckx, S.; Goovaerts, E.; Wenseleers, W. Experimental observation of single-file water filling of thin single-wall carbon nanotubes down to chiral index (5,3). *Phys. Rev. Lett.* **2010**, *104*, 207401.

[26] Dresselhaus, M. S.; Jorio, A.; Souza Filho, A. G.; Saito, R. Defect characterization in graphene and carbon nanotubes using Raman spectroscopy. *Philos. Trans. R. Soc., A* **2010**, *368*, 5355-5377.

[27] Miyata, Y.; Mizuno, K.; Kataura, H. Purity and defect characterization of single-wall carbon nanotubes using Raman spectroscopy. *J. of Nanomater.* **2011**, *2011*.

[28] Liu, H.; Tanaka, T.; Urabe, Y.; Kataura, H. High-efficiency single-chirality separation of carbon nanotubes using temperature-controlled gel chromatography. *Nano Lett.* **2013**, *13*, 1996-2003.

[29] D'Alagni, M.; D'Archivio, A. A.; Galantini, L.; Giglio, E. Structural study of the micellar aggregates of sodium chenodeoxycholate and sodium deoxycholate. *Langmuir* **1997**, *13*, 5811-5815.

[30] Glaeske, M.; Setaro, A. Nanoplasmonic colloidal suspensions for the enhancement of the luminescent emission from single-walled carbon nanotubes. *Nano Res.* **2013**, *6*, 593-601.

[31] Shea, M. J.; Arnold, M. S. 1% solar cells derived from ultrathin carbon nanotube photoabsorbing films. *Appl. Phys. Lett.* **2013**, *102*, 243101.

[32] Wang, C.; Zhang, J.; Ryu, K.; Badmaev, A.; De Arco, L. G.; Zhou, C. Wafer-scale fabrication of separated carbon nanotube

thin-film transistors for display applications. *Nano Lett.* **2009**, *9*, 4285-4291.

[33] Zhang, J.; Gui, H.; Liu, B.; Liu, J.; Zhou, C. Comparative study of gel-based separated arcdischarge, HiPCO, and CoMoCAT carbon nanotubes for macroelectronic applications. *Nano Res.* **2013**, *6*, 906-920.

[34] Diao, S.; Hong, G.; Robinson, J. T.; Jiao, L.; Antaris, A. L.; Wu, J. Z.; Choi, C. L.; Dai, H. Chirality enriched (12,1) and (11,3) single-walled carbon nanotubes for biological imaging. *J. Am. Chem. Soc.* **2012**, *134*, 16971-16974.

[35] Hong, G.; Lee, J. C.; Robinson, J. T.; Raaz, U.; Xie, L.; Huang, N. F.; Cooke, J. P.; Dai, H. Multifunctional *in vivo* vascular imaging using near-infrared Fluorescence. *Nature Med* **2012**, *18*, 1841-1846.

[36] Behabtu, N.; Young, C. C.; Tsentalovich, D. E.; Kleinerman, O.; Wang, X.; Ma, A. W. K.; Bengio, E. A.; ter Waarbeek, R. F.; de Jong, J. J.; Hoogerwerf, R. E.; *et al*. Strong, light, multifunctional fibers of carbon nanotubes with ultrahigh conductivity. *Science* **2013**, *339*, 182-186.

[37] Wu, M.; Liu, K.; Wang, W.; Sui, Y.; Bai, X.; Wang, E. Ultralong aligned single-walled carbon nanotubes on flexible fluorphlogopite mica for strain sensors. *Nano Res.* **2012**, *5*, 443-449.

[38] Tenent, R. C.; Barnes, T. M.; Bergeson, J. D.; Ferguson, A. J.; To, B.; Gedvilas, L. M.; Heben, M. J.; Blackburn, J. L. Ultrasmooth, large-area, high-uniformity, conductive transparent single-walled carbon nanotube films for photovoltaics produced by ultrasonic spraying. *Adv. Mater.* **2009**, *21*, 3210-3216.

[39] Wang, Y.; Huang, L.; Liu, Y.; Wei, D.; Zhang, H.; Kajiura, H.; Li, Y. Minimizing purification-induced defects in single-walled carbon nanotubes gives films with improved conductivity. *Nano Res.* **2009**, *2*, 865-871.

[40] Zhao, S.; Kitagawa, T.; Miyauchi, Y.; Matsuda, K.; Shinohara, H.; Kitaura, R. Rayleigh scattering studies on inter-layer interactions in structure-defined individual double-wall carbon nanotubes. *Nano Res.* **2014**, *7*, 1548-1555.

[41] Cambré, S.; Santos, S. M.; Wenseleers, W.; Nugraha, A. R. T.; Saito, R.; Cognet, L.; Lounis, B. Luminescence properties of individual empty and water-filled single-walled carbon nanotubes. *ACS Nano* **2012**, *6*, 2649-2655.

[42] Cambré, S.; Wenseleers, W. Separation and diameter-worting of empty (end-capped) and water-filled (open) carbon nanotubes by density gradient ultracentrifugation. *Angew. Chem. - Int. Ed.* **2011**, *50*, 2764-2768.

[43] Fagan, J. A.; Becker, M. L.; Chun, J.; Hobbie, E. K. Length fractionation of carbon nanotubes using centrifugation. *Adv. Mater.* **2008**, *20*, 1609-1613.

[44] Wu, Z.; Chen, Z.; Du, X.; Logan, J. M.; Sippel, J.; Nikolou, M.; Kamaras, K.; Reynolds, J. R.; Tanner, D. B.; Hebard, A. F.; *et al*. Transparent, conductive carbon nanotube films. *Science* **2004**, *305*, 1273-1276.

[45] Zhu, Y.; Murali, S.; Cai, W.; Li, X.; Suk, J. W.; Potts, J. R.; Ruoff, R. S. Graphene and graphene oxide: synthesis, properties, and applications. *Adv. Mater.* **2010**, *22*, 3906-3924.

Electronic Supplementary Material

Benchtop aqueous two-phase extraction of isolated individual single-walled carbon nanotubes

Navaneetha K. Subbaiyan,[1,†] A. Nicholas G. Parra-Vasquez, [1,†] Sofie Cambré,[1,2,†] Miguel A. Santiago Cordoba,[1] Sibel Ebru Yalcin,[1] Christopher E. Hamilton,[1] Nathan H. Mack,[1] Jeffrey L. Blackburn,[3] Stephen K. Doorn,[1] and Juan G. Duque[1](✉).

[1] *Chemistry Division, Physical Chemistry and Applied Spectroscopy Group (C-PCS), Center for Integrated Nanotechnologies (CINT), and Materials Science & Technology Division (MST-7), Los Alamos National Laboratory, Los Alamos, New Mexico 87544, United States.* [2] *Experimental Condensed Matter Physics Laboratory, University of Antwerp, Antwerp, B-2610, Belgium*

[3] *National Renewable Energy Laboratory, Golden, Colorado 80401, United States*

[†] *These authors contributed equally*

Supporting information to DOI 10.1007/s12274-****-****-* (automatically inserted by the publisher)

S1: Materials

Table – S1: – Various SWCNT source materials used in this study. The diameter range was extracted from absorption spectra.

Name	Manufacturer	Batch	Diameter range
HiPco	Rice University	195.2	d=0.9 ±0.3 nm
CoMoCat SG65i	SWeNT	SG65i-L39	d=0.7 ±0.1 nm
Laser Vaporization	NREL	Y140307	d=1.2 ±0.2 nm
Plasma Torch	Raymor	RNL12-010-113	d=1.3 ±0.2 nm
Arc-discharge 1	Simga Aldrich	07826BA	d=1.4 ±0.2 nm
Arc-discharge 2	Nanoledge	P00508D	d=1.5 ±0.2 nm

S2: Methods

S2.a. Optical Absorption Spectroscopy and Volume Dilution Correction

Absorption spectra were recorded with a UV-vis-NIR spectrophotometer (Cary 6000i) in the range of 200-1700nm (H_2O-samples) and with a Cary 5E spectrophotometer in the range of 175-2500nm (D_2O-samples), using fused silica cells with an optical path length of 1 cm or 3 mm. Spectra were diluted if necessary (to keep OD < 3) and afterwards rescaled according to their dilution factor and to a 1mm optical path length.

For proper comparison of the separation yields, absorption spectra were rescaled according to their volumetric dilutions as in our previous work.[20]

We start with a mass balance:

$$M_P = M_T + M_B + M_I \quad (1)$$

where is the mass of the SWCNTs in the parent dispersion (P), top phase (T), bottom phase (B) and the interface (I). The mass can be determined from absorption through an extinction coefficient, ε:

$$M_j = \frac{a_j}{\varepsilon_j} V_j \quad (2)$$

where a_j is absorption and V_j is the volume of the respective dispersion. Assuming the extinction coefficient does not change significantly in each fraction, equation (1) can be rearranged to compare absorbances:

$$a_P = \frac{V_T}{V_P} a_T + \frac{V_B}{V_P} a_B + \Delta Q \quad (3)$$

where ΔQ is the loss of material at the interface. For multi-chiral separation: V_S =400μL, V_B =1180μL and V_T=3540μL.

S2.b. 2D IR fluorescence-excitation (PLE) spectroscopy

2D IR band-gap PLE spectra were recorded using a home-built spectrometer: the sample was excited with a pulsed Xe-lamp (Edinburgh Instruments, Xe900-xP920), and excitation wavelengths were spectrally selected with a 300mm grating monochromator (Acton SpectraPro 2355). Emission was collected at 90° and analyzed using a 150 mm grating spectrograph (Acton SpectraPro 2156) with a liquid nitrogen cooled extended InGaAs photodiode array detector (Princeton Instruments OMA V:1024/LN-2.2), sensitive up to 2.2 μm. Spectra were recorded with 5 nm steps in excitation wavelength and an instrumental resolution of 8 nm in excitation and 10 nm in emission wavelength. Appropriate filters were used to eliminate stray light and higher order diffractions from the spectrometers, and all spectra were corrected for detector and spectrograph sensitivity, filter transmission, and (temporal and spectral) variations of the excitation light intensity.

S2.c. Resonant Raman spectroscopy

Resonant Raman spectra were excited at multiple laser wavelengths originating either from a Kr+- ion laser, or from a tunable Rhodamine 6G dye or Ti:Sapphire laser both pumped by an Ar+- ion laser. Spectra were recorded in backscattering geometry using either a 5-5-5 Princeton Instruments Trivista or a Dilor XY800 triple Raman spectrometer.

S2.d. Transmission electron microscopy (TEM)

All TEM samples were prepared by dropping ~2 micro liters of SWCNT solutions onto a lacey carbon coated copper TEM foil. The solution was allowed to wick into a filter paper below and the grid was rinsed with DI water. All samples were imaged on a FEI Tecnai F30 operated at 300kV.

S2.e. Thermo gravimetric analysis (TGA)

20 ml of solution (ATP separated SWCNT dispersion from bottom phase) is filtered and rinsed to remove surfactants using 0.2 μm pore diameter membrane (polycarbonate). Resulting 2 mg of the SWCNTs and 2 mg of raw SWCNTs were used for recording TGA (Thermal Analysis TGA, Q500). The heating rate used was 5°C/min and heated up to 800°C in air.

S2.f. Atomic force microscope (AFM)

Atomic force microscope (AFM) images were obtained with a Nanoscope IV (Digital Instruments/Veeco/Bruker Metrology, Inc., SantaBarbara, CA), operating in tapping mode, using an ultrasharp N-type silicon tip coated with Al on its reflective side for better laser signal quality (APP Nano ACTA, 0.01 – 0.025 ohm/cm, < 10 nm radius, f: 200 – 400 kHz, k: 25 -75 N/m) at a scan-rate of 0.6 Hz and 512 x 512 resolution. Samples for AFM analysis were prepared with 20 μL of SWNT suspensions spin coated at 5000 RPM onto roughly 0.4 cm² freshly cleaved mica surfaces(Ted Pella, Inc., Redding, CA) and rinsed with 2-isopropanol

while spinning to remove the excess of surfactant. Samples were left spinning for 10 min to dry thoroughly.

S2.g. Photoluminescence (PL) images

Individual SWCNT PL images were acquired using an inverted microscope coupled to an EMCCD (Princeton Instruments ProEM 512). The excitation laser light at 568 nm (Coherent Sapphire LP) was focused on the back aperture of a 1.49 NA, 100x microscope objective to achieve a wide field imaging spot size of ~20 μm. Individual SWCNT PL was collected through the same objective and imaged on the EMCCD. 100μL of strongly diluted separated SWCNT dispersions were mixed with 10μL of tetramethylorthosilicate (TMOS). 10μL of this TMOS-SWCNT dispersion was sandwiched between acid- and plasma-cleaned quartz slides (EscoOptics). PL images were obtained with 1 second exposure time.

S3. Additional Figures

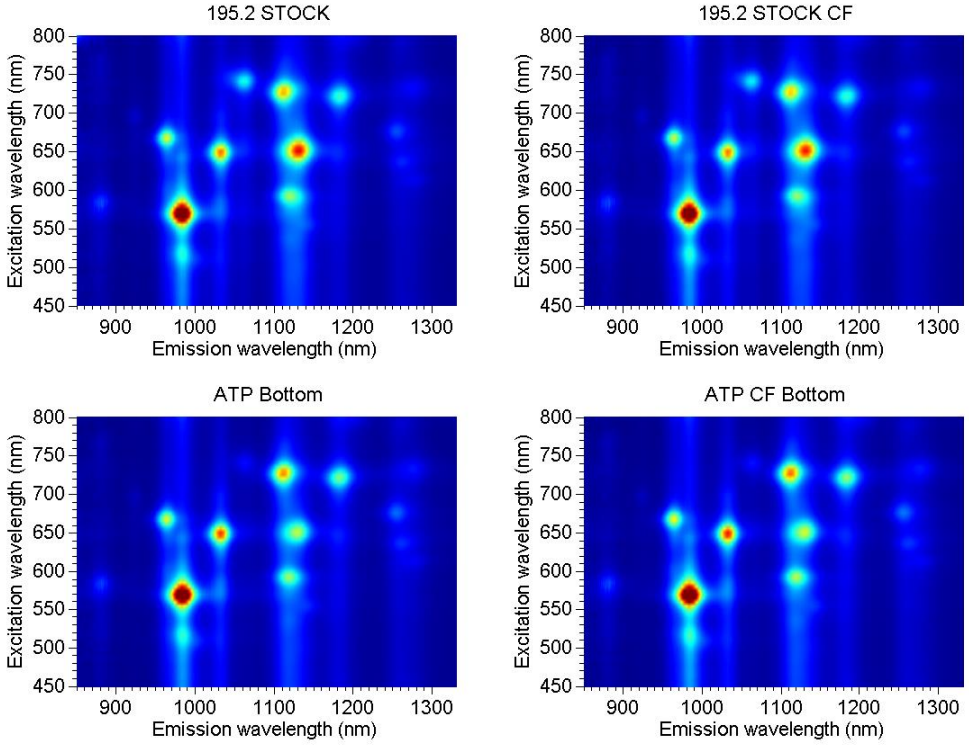

Figure S1: PLE maps before and after ATP separation. PLE maps of the starting HiPco 195.2 dispersion, the dispersion after CF, and the ATP bottom phases before and after CF of the parent solution, showing that the SWCNT chirality distribution remains the same in all samples. Spectra were calibrated for excitation light intensity and detector sensitivity.

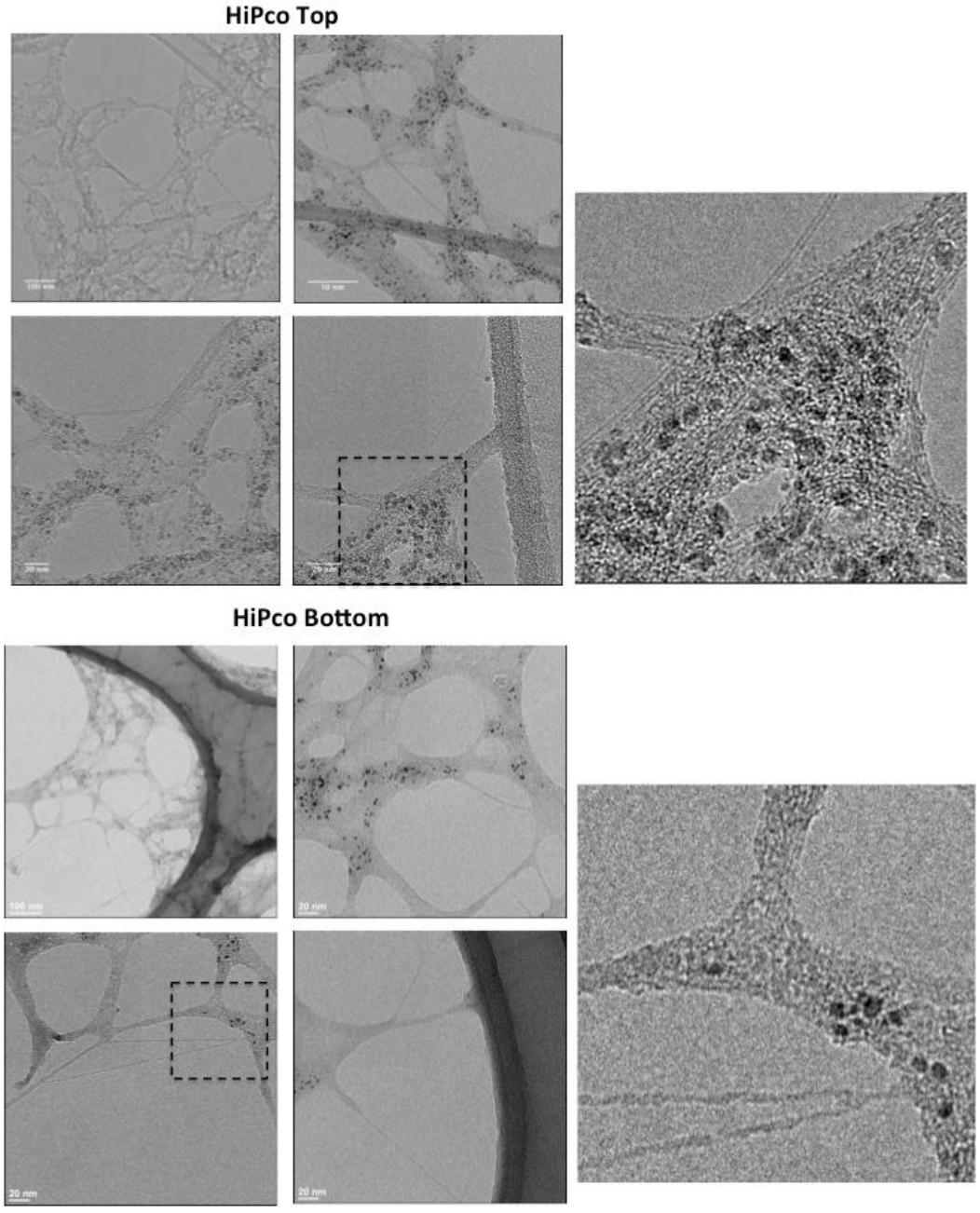

Figure S2: TEM HiPco top and bottom: Less amount of catalyst in the bottom phase.

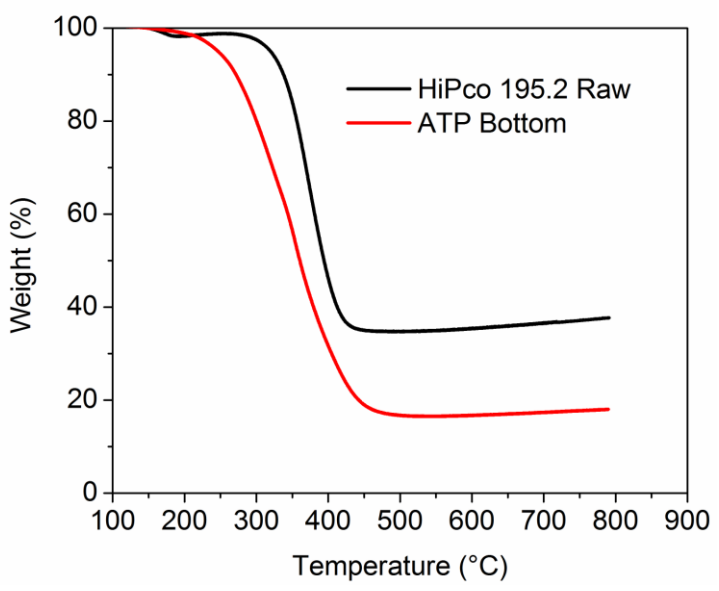

Figure S3: TGA analysis before and after separation. TGA analysis obtained in air for the starting as-received HiPco 195.2 SWCNTs and the separated ATP-bottom phase shows that along with bundles, a significant fraction of catalyst particles are removed. For the TGA analysis, the ATP bottom fraction was first rinsed sufficiently with H_2O to remove remaining dextran, PEG and surfactants.

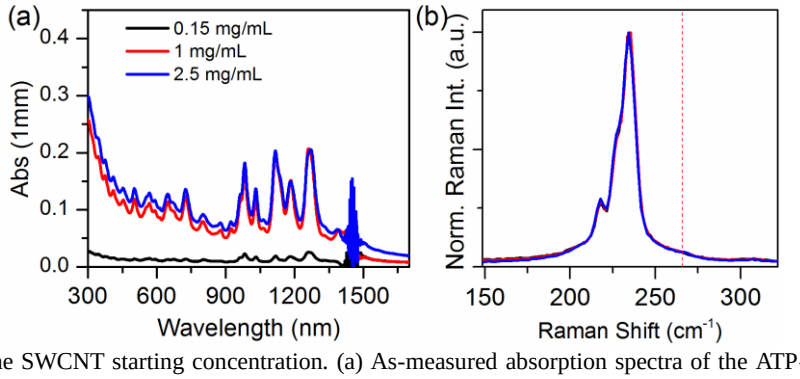

Figure S4: Variation of the SWCNT starting concentration. (a) As-measured absorption spectra of the ATP-separated bottom phase for 3 different starting concentrations of the parent dispersion. (b) Resonant Raman spectra excited at 785nm, showing no presence of a (10,2)-bundle Raman vibration in these bottom fractions (dashed red line indicates the expected position). Only a rescaling of the overall intensity is observed, as the concentration of isolated SWCNTs decreases for a smaller SWCNT starting concentration.

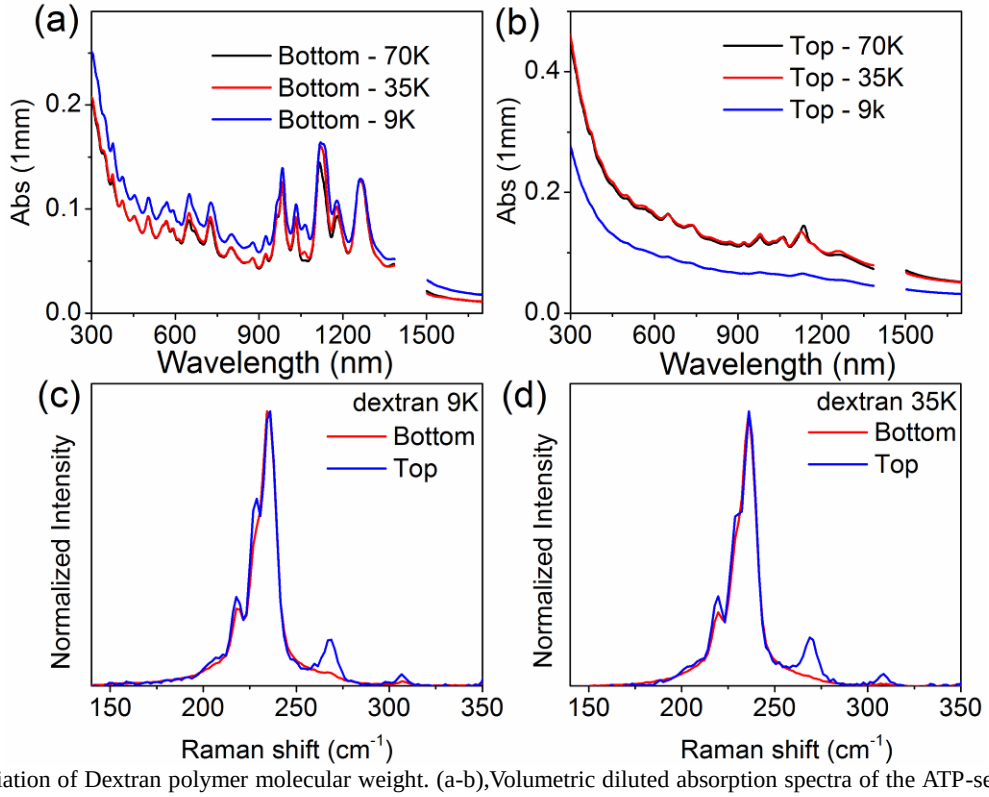

Figure S5: Variation of Dextran polymer molecular weight. (a-b),Volumetric diluted absorption spectra of the ATP-separated bottom (a) and top (b) phases for different dextran MW at a fixed DOC concentration of 0.088%wt/V. (c-d) Resonant Raman spectra excited at 785nm, showing the presence of a (10,2)bundle RBM only visible at this wavelength when bundles are present for top and bottom phases separated using dextran 9K (nominal 9-11K) (c) and dextran 35K (nominal 35-45K) (d). Notice that as the MW of dextran decreases, relatively more SWCNTs are separated into the bottom phase (including bundles, as is expected for any particles that are separable with ATP), however, by slightly lowering the DOC concentration, these bundles can be removed to the top phase or interface.

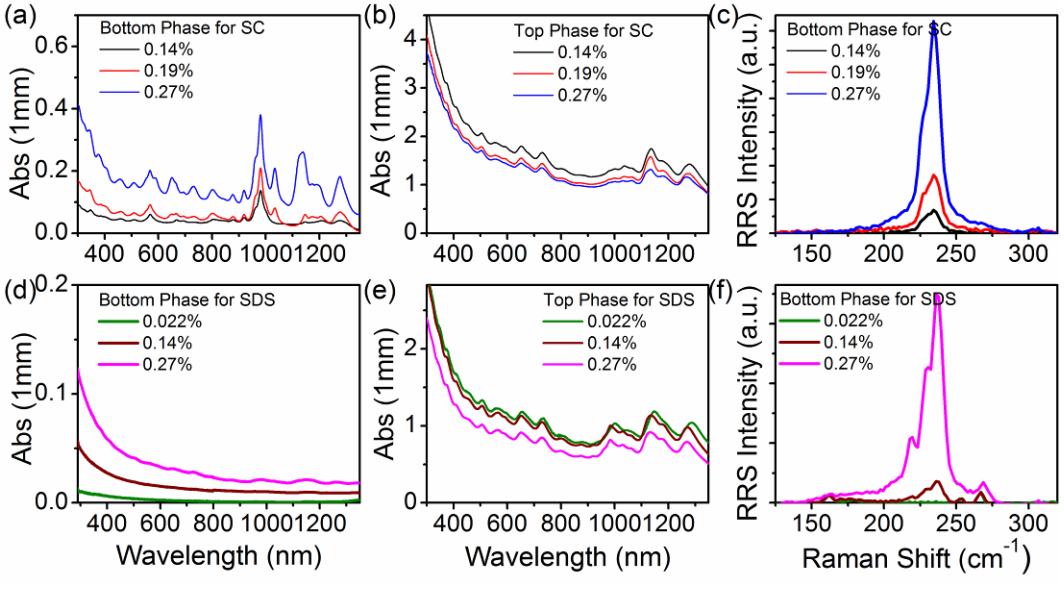

Figure S6: Variation of SC and SDS concentration. Absorption spectra of bottom (a and d) and top (b and e) phases for SC (a-b) and SDS (d-e) rescaled according to their volumetric dilutions, combined with RRS spectra (c and f) of the bottom phases to study the presence of bundles. For SC, multi-chiral separation can be achieved only at higher surfactant concentration, while for lower concentration the distribution of SWCNTs is skewed toward small diameters. For SDS, even sufficiently high surfactant concentration does not allow the SWCNTs to distribute into the bottom phase, without the presence of bundles or other impurities.

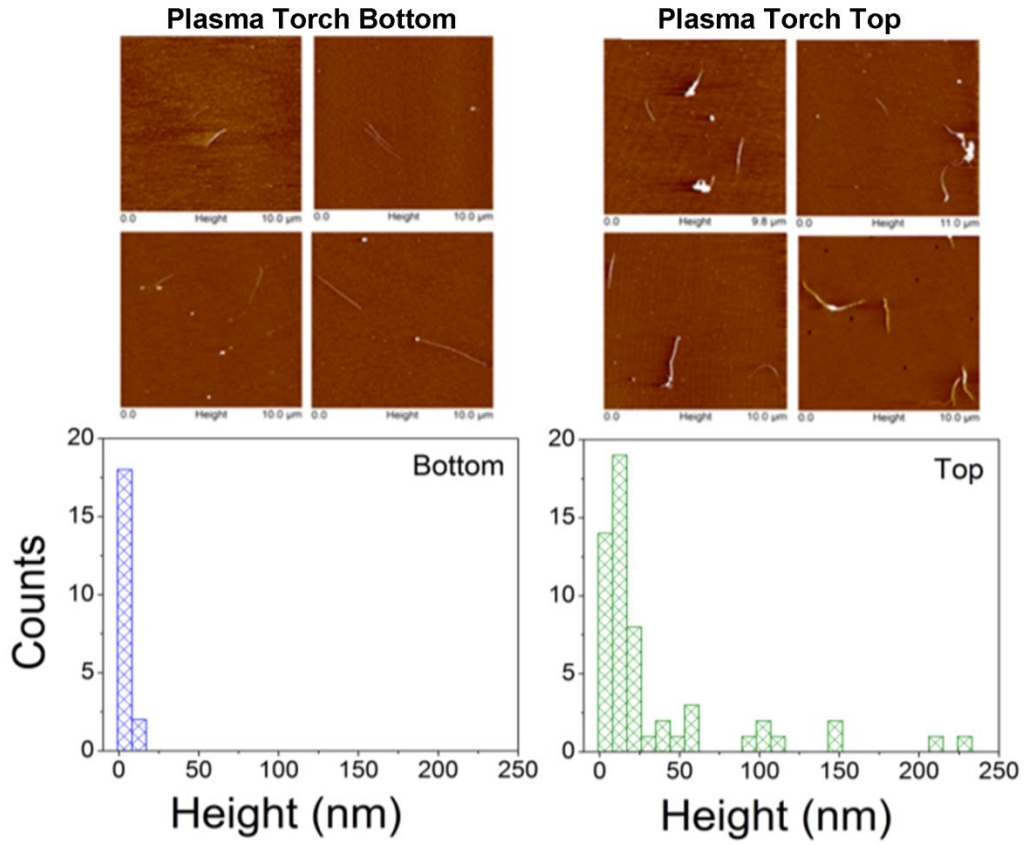

Figure S7: AFM images of Plasma Torch top and bottom fractions. Significant number of SWCNT bundles in the top phase in comparison to the bottom phase for both types of dispersions

.

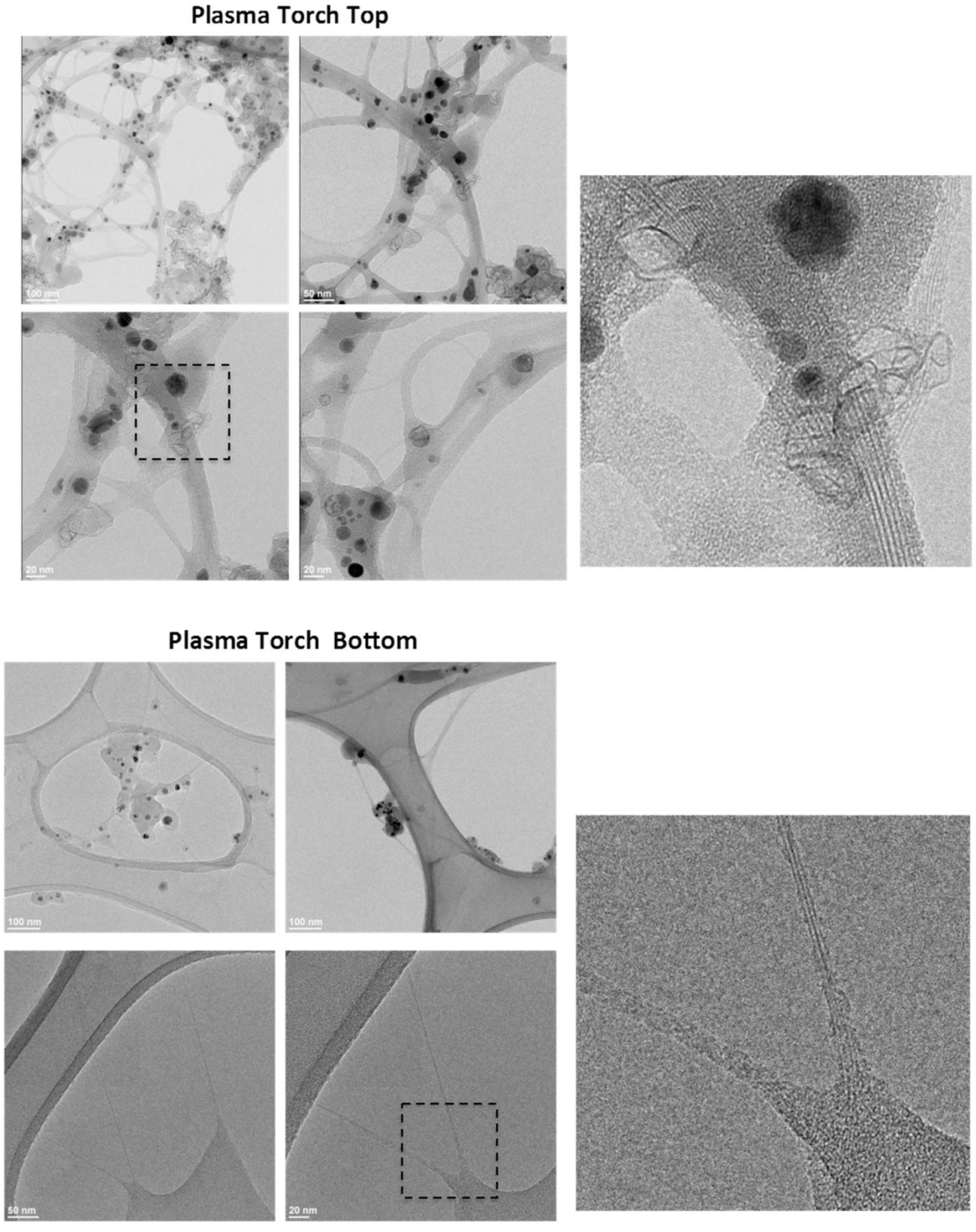

Figure S8:TEM Plasma Torch top and bottom fractions. Less amount of catalyst and carbonaceous materials in the bottom phase than in the top

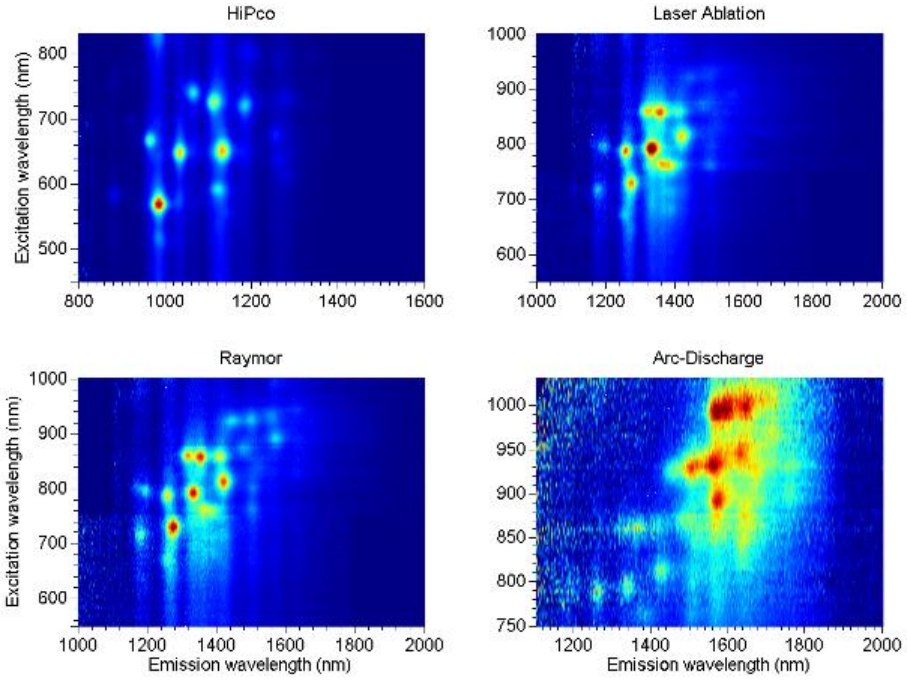

Figure S9: PLE of separated ATP bottom fractions. Multichiral separation from different CNT sources resulted in highly resolved PLE maps, even for the larger diameter SWCNTs. Spectra were calibrated for excitation light intensity and detector sensitivity

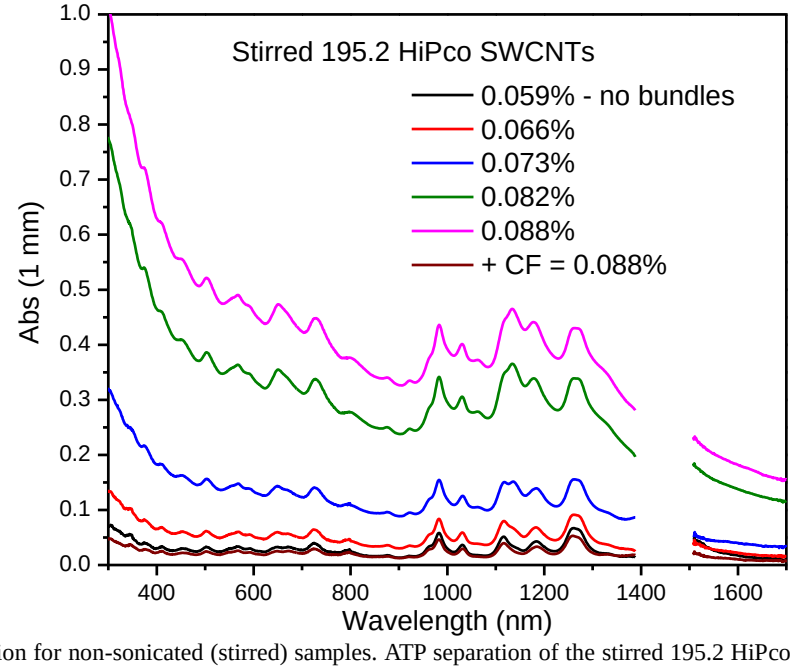

Figure S10: ATP separation for non-sonicated (stirred) samples. ATP separation of the stirred 195.2 HiPco dispersion using different DOC concentrations for the non-centrifuged sample (rescaled for volumetric dilution). While after centrifugation (e.g. 2h at 40000g or 4h at 16000g) the normal 0.088%wt/V of DOC is sufficient, before centrifugation 0.059%wt/V yields identical separation. We believe the lower DOC concentration is necessary because of a much higher bundle content (relative to the actual DOC concentration) in the parent suspension.

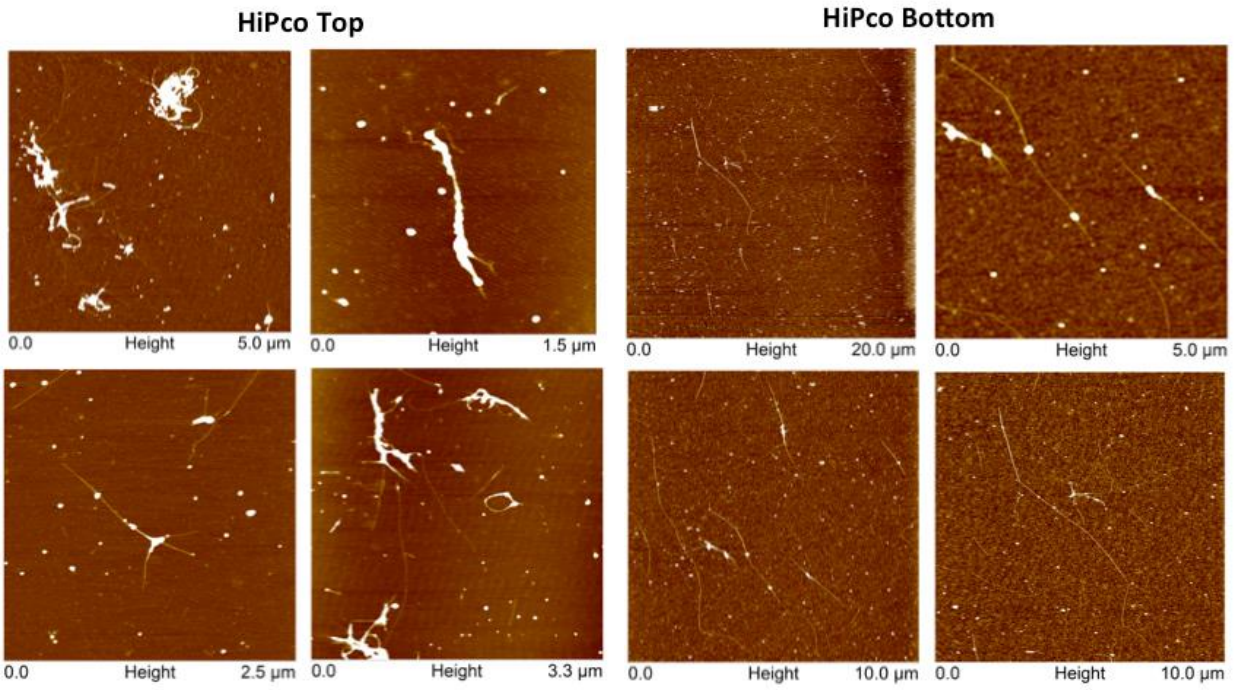

Figure S11: AFM images of HiPco top and bottom fractions after stirring. Significant number of SWCNT bundles in the top phase in comparison to the bottom phase and relatively long SWCNTs in the bottom phase can be observed.

Address correspondence to J. G. Duque, jduque@lanl.gov